

ASCA Observations of a Nearby and Massive Galaxy Cluster, Abell 3627

Takayuki TAMURA, Yasushi FUKAZAWA, Hidehiro KANEDA, Kazuo MAKISHIMA, Makoto TASHIRO

Department of Physics, School of Science, The University of Tokyo, Hongo, Bunkyo-ku, Tokyo 113-0033

E-mail(TT): ttamura@amalthea.phys.s.u-tokyo.ac.jp

Yasuo TANAKA*

The Institute of Space and Astronautical Science, 3-1-1 Yoshinodai, Sagami-hara, Kanagawa 229-8510

and

Hans BÖHRINGER

Max-Planck-Institut für extraterrestrische Physik, D-85740 Garching, Germany

(Received 1997 April 16; accepted 1998 February 23)

Abstract

The results obtained from ASCA observations of the cluster of galaxies Abell 3627 are presented. This cluster, located behind the Milky Way, was recently found to be a nearby, X-ray bright and very rich cluster. Pointed observations onto the central region of the cluster gave a gas temperature of ~ 7 keV and a metallicity of about 0.2 solar. An offset pointing to a substructure elongated to the south-east of the cluster center gave a significantly lower temperature of ~ 5 keV. The 2–10 keV luminosity within a radius of $40'$ (1.1 Mpc) is estimated to be 3.7×10^{44} erg s $^{-1}$. The X-ray data imply a cluster mass of about $4 \times 10^{14} M_{\odot}$ within $40'$.

Key words: Galaxies: abundances — Galaxies: clustering — Galaxies: clusters: individual: (Abell 3627) — X-rays: galaxies

* Present address: Max-Planck-Institut für extraterrestrische Physik, D-85740 Garching, Germany

1. Introduction

Abell 3627 (hereafter A3627) was recently found to be a nearby ($z = 0.016$), very rich cluster behind the southern Milky Way by Kraan-Korteweg et al. (1996). Although it was catalogued as a nearby rich cluster in the ACO catalog (Abell et al. 1989), this cluster had received little attention before. This is partly because of a high degree of galactic obscuration towards the cluster direction of $(l, b) = (325^\circ, -7^\circ)$. The galaxy velocity dispersion of $\sigma = 897 \text{ km s}^{-1}$ from a redshift survey (Kraan-Korteweg et al. 1996) indicates the gravitational mass of A3627 to be $5.1 \times 10^{15} M_\odot$, which is comparable to that of the Coma cluster, and is typical of a rich cluster. The direction and distance of A3627 are also interesting, because the implied position falls near to the location predicted for the center of the Great Attractor (Lynden-Bell et al. 1988), suggesting that the cluster lies near the bottom of the Attractor's gravitational potential well.

This cluster had escaped X-ray detection in the previous surveys, and was first discovered by the ROSAT All Sky Survey as one of the brightest clusters in X-rays. A follow-up pointed observation with the ROSAT PSPC by Böhringer et al. (1996; hereafter B96) showed that the cluster is indeed very massive in both gas mass and gravitational mass. The PSPC image shows that the cluster is elongated to the south-east direction. The X-ray morphology of the cluster can be interpreted as a merger where a smaller cluster in the south-east part is colliding with the main cluster (B96). According to a PSPC observation (B96), the X-ray luminosity in 0.1–2.4 keV and the gas temperature are $(2.2 \pm 0.3) \times 10^{44} h_{50}^{-2} \text{ erg s}^{-1}$ and 5–10 keV, respectively, where the Hubble constant is expressed as $H_0 = 50 h_{50} \text{ km s}^{-1} \text{ Mpc}^{-1}$. However, the limited energy band of ROSAT and a large interstellar hydrogen column (around $1.8 \times 10^{21} \text{ cm}^{-2}$) prevented accurate determinations of the X-ray spectroscopic properties.

We observed the central regions of A3627 with ASCA (Tanaka et al. 1994) in the energy band of 0.5–10 keV. In this article we report on the results of the properties of A3627 obtained from these observations, and compare them with those of other nearby rich clusters of galaxies.

2. Observations and Results

2.1. Observations

The ASCA X-ray telescope (XRT; Serlemitsos et al. 1995) was pointed at the center of the cluster on 1996 February 27 and 28, and 19' south-east from the center on 1996 February 29. Hereafter, we refer to these two pointings as

CENTER and SE. The pointing directions were $16^{\text{h}}15^{\text{m}}44^{\text{s}}, -60^{\circ}49'56''$ (J2000) and $16^{\text{h}}17^{\text{m}}25^{\text{s}}, -61^{\circ}4'13''$ (J2000) during the CENTER and SE observations, respectively. The observations were performed with the SIS (Solid-state Imaging Spectrometer; Burke et al. 1994) in the 2-CCD faint/bright mode and the GIS (Gas Imaging Spectrometer; Ohashi et al. 1996) in the PH normal mode. We have screened events by using standard data-selection criteria; i.e., geomagnetic cutoff rigidity > 6 and $> 8 \text{ GeV } c^{-1}$ for the SIS and GIS, respectively, the elevation angle above the earth's horizon $> 10^{\circ}$ for the GIS, and $> 10^{\circ}$ (dark earth) or $> 25^{\circ}$ (sunlit earth) for the SIS. The thus-obtained net exposure times for the CENTER pointing are ~ 29 ks with the SIS and ~ 37 ks with the GIS, while those for SE are ~ 26 ks with the SIS and ~ 25 ks with the GIS.

2.2. *The X-Ray Image*

The GIS count rates in 0.7–10 keV within the entire field of view were $2.5 \text{ c s}^{-1}/\text{detector}$ for the CENTER pointing and $1.2 \text{ c s}^{-1}/\text{detector}$ for the SE pointing. These include background of $0.2 \text{ c s}^{-1}/\text{detector}$. Figure 1 shows the background-subtracted mosaic X-ray image of A3627, obtained with the GIS (GIS 2+GIS 3) from the two pointings. The image was corrected for the exposure time, but not for the vignetting or the supporting grids of the GIS window. The X-ray brightness centroid is near to the radio galaxy PKS 1610–60, which is one of the three bright central galaxies of the cluster (B96), and has relatively large radio lobes. The overall X-ray morphology is not circularly symmetric, as already recognized in the ROSAT image (B96). The X-ray emission of the cluster almost fills the entire GIS fields of view of the two pointings and can be observed out to at least $40'$ ($1.1 h_{50}^{-1} \text{ Mpc}$) toward the south-east direction from the center. In the ROSAT observations, the cluster X-ray emission is found up to a radius of 1° (B96).

2.3. *The X-Ray Spectra*

In order to study the spatially averaged properties of the X-ray emission, we first utilized the data obtained with the GIS, which cover a larger field of view compared to that of the SIS. We accumulated the GIS events from the two detectors (GIS 2 and GIS 3) within a circle having a projected radius of $14'$, one for each pointing, as shown in figure 2 as G-a and G-b. The background spectrum was obtained from the “blank-sky” (containing no bright sources) database by extracting the events within an identical region for the same detector. The thus-derived GIS spectra are shown in figure 3, without any correction for the energy-dependent instrument response. The circle for

the CENTER region includes PKS 1610–60. However, its contribution is estimated to be $\sim 1\%$ of the total photon number from the PSPC observation; hence, the effect to the observed spectrum is negligible.

We fitted the GIS spectra in 0.7–10.0 keV with an isothermal Raymond-Smith (1977) plasma model including the photoelectric absorption. As shown in table 1 and illustrated in figure 3, the fits are generally acceptable. The result shows that the temperature in the SE region is lower than that in the CENTER region by about 2 keV. We find that the best-fit hydrogen-column densities are lower than the published galactic value of $1.8 \times 10^{21} \text{ cm}^{-2}$ towards A3627 obtained from the 21cm observations (Stark et al. 1992). We return to this problem later.

Here, we should note that the obtained spectra contain the effect of the stray light, i.e. photons scattered in from regions outside of the fields of view. Although the stray light from the outer region to the CENTER region is negligible, that from the central region to the SE region accounts for about 15% of the observed flux. In order to correct for this effect, we estimated the spectrum of the stray light from the central region to the SE region by a ray-tracing simulation (Honda et al. 1996) employing the β model brightness distribution derived from the ROSAT observations ($\beta = 0.56$ and a core radius of $r_c = 10'.0$; B96). By subtracting the thus-estimated stray spectrum of the contamination, we fitted the spectrum of the SE region again. The temperature of the SE region turned out to be 4.0–5.3 keV. This range is consistent with, but even lower than, that given in table 1. Therefore, we conclude that the SE region has a lower temperature than the CENTER region, even when taking into account the effects of stray light.

We next utilized the data from the SIS, which has a higher sensitivity at lower energies, hence allowing a more accurate determination of N_{H} . We accumulated the SIS events within a circle of a projected radius $4'.9$, one from CENTER and two from SE, as shown in figure 2. We fitted the same model to the SIS spectra as that used for the GIS spectra. As shown in table 1 and illustrated in figure 4, the fits are acceptable, yielding the best-fit N_{H} values in the range $1.3 - 2.0 \times 10^{21} \text{ cm}^{-2}$. Within the statistical uncertainties, these are consistent with the above-mentioned galactic value, and also with the ROSAT PSPC result for which the 90% limits span a range of $1.4 - 1.9 \times 10^{21} \text{ cm}^{-2}$ (B96). We consider that the lower values of N_{H} derived from the GIS spectra are probably due to a calibration uncertainty in the low-energy response of the GIS. The temperature and metallicity derived from the SIS are fully consistent with those from the GIS, though with slightly larger errors.

The metallicity values determined from the iron K-line for different regions (table 1) are consistent with one another, showing a fairly uniform metallicity throughout the whole cluster. To better determine the metallicity

around the cluster center, we fitted the spectra within a circle of radius of $5'$ from the cluster center of the GIS and the SIS jointly with the isothermal plasma model. As a result, the 90% confidence limit of the metallicity was found to be 0.18–0.26 solar. We also obtained the 90% confidence limit of the temperature from a joint fit to be 6.4–6.9 keV.

The 2–10 keV luminosity within a radius of $40'$ was estimated to be $3.7 \times 10^{44} h_{50}^{-2}$ erg s $^{-1}$ after correcting for absorption. For this calculation we employed the spatial gas distribution derived from the ROSAT PSPC observations (B96) and the best-fit spectral model which we mentioned above.

3. Discussion

We derived the X-ray luminosity and the gas temperature in the central region of A3627 using the broad-band imaging spectroscopic data of ASCA.

A temperature of 6.7 ± 0.3 keV, found in the CENTER region, is consistent with a velocity dispersion of 897 km s $^{-1}$ by Kraan-Korteweg et al. (1996). The ratio of the specific energy in galaxies to that in the hot gas, $\beta_{\text{spec}} = 0.82$, is a typical value for clusters (Edge et al. 1991). The X-ray luminosity versus temperature of A3627 is also in general agreement with the empirical correlation between these two quantities (David et al. 1993). Assuming that the cluster has an isothermal and spherically symmetric gas distribution, the temperature measured in the CENTER region gives a gravitational mass of $4 \times 10^{14} h_{50}^{-1} M_{\odot}$ within $40'$ ($1.1 h_{50}^{-1}$ Mpc) and a gas mass fraction (ratio of the gas mass to the total mass) of $11 h_{50}^{-1.5}\%$. Here, we used again the gas-distribution model from the ROSAT observations (B96). The gravitational mass of the main cluster extrapolated to 3 Mpc, which is approximately the virial radius of this galaxy system, is about $10^{15} M_{\odot}$ within an uncertainty of about a factor of 2. Thus, the main component turns out to have about half the mass of the Coma cluster. The substructure extending to the south-east direction may add up to 50% to the total cluster mass. This total cluster mass is several times lower than that estimated from the galaxy velocity dispersion by Kraan-Korteweg et al. (1996). However, this is not a discrepancy, but is simply because their mass refers to a much larger volume.

We found that the temperature of the SE region, 4.0 – 5.3 keV, is significantly lower than that of the CENTER region, which confirms the temperature drop in the south-east direction from the cluster center previously noted by B96. The temperature difference suggests that there is a systematic temperature drop toward the outer region, or that the SE region is a substructure that is cooler than the main cluster. The agreement of the average temperature

within 14' radius with that for the central 5' radius supports a uniform temperature distribution in the main cluster within the observed scale. Therefore, the lower temperature seems to be a particular property of the SE region, which is coincident with the substructure in the X-ray brightness distribution (B96). Based on the morphology, Böhringer et al. (B96) suggested that this substructure is a subcluster in the process of merging with the main cluster.

Together with the imaging data (B96), we may attempt to interpret the nature of the merger configuration. The projected distance of the two merging subunits is about $(0.5 - 0.6) h_{50}^{-1}$ Mpc. If the inclination angle between the sky plane and the merger axis is not very large, the two merging units are already in close contact. In principle, there are three alternative possibilities: (1) the merging subunit is on its first infall and not yet affected by the resulting shock; (2) the infalling subunit is already subject to shock heating; or (3) the two units have already passed each other. In the last case, after the core collision, there is a rebound phase which can lead to a separation of the two merging units on the order of $1 h_{50}^{-1}$ Mpc at turnaround (e.g. Burns et al. 1994).

In the first case, the two units are expected to behave as two independent clusters, following individually the normal luminosity (L_X) versus temperature (T) scaling of $L_X \propto T^3$ (e.g., David et al. 1993). However, the observed flux ratio between the main and sub components, approximately $7 - 10 : 1$, is much larger than the ratio of ~ 3 predicted by their temperature ratios. Therefore, this possibility may be unlikely. However, in the third case the subcomponent has already passed through the main cluster center, and the subcomponent gas was heated and reassembled in the subcluster potential (see e.g. Schindler, Müller 1993; Kulp 1998). In this case, it is not surprising that the two temperatures are comparable. However, the merging subunit in the south-east still appears to be fairly compact, and the central radio-lobe galaxy does not exhibit much disturbance. Therefore, this alternative is not very likely, either. Thus, by elimination, the second possibility is the most plausible.

Honda et al. (1996) also found a significant temperature variation in the Coma Cluster. It is interesting to note that its prominent subcluster in the south-west direction, centered on NGC 4839, also shows a lower temperature than that of the cluster average. Another low-temperature region of the Coma cluster in the south-east actually coincides with a substructure associated with a bright elliptical NGC 4911. This is one of the clear substructural features noted by Briel et al. (1992) and later by others (White et al. 1993; Vikhlinin et al. 1997). These facts appear to be similar to the case of A3627.

The ASCA observations enabled us to determine the metallicity of the ICM of A3627 for the first time. The

spatially averaged metallicity of 0.16–0.31 solar agrees with the typical values of 0.15–0.3 solar in rich clusters, including the Coma cluster, observed with Ginga (Hatsukade 1989) and with ASCA (e.g., Fukazawa et al. 1997). The results from the CENTER and SE regions are consistent with a uniform abundance distribution over the entire cluster. We found no significant metallicity increase toward the center of the cluster, which had been found in some low-temperature clusters, particularly those containing cD galaxies (Koyama et al. 1991; Fukazawa et al. 1994; Xu et al. 1997; Ezawa et al. 1998).

It is quite interesting that we found this very massive cluster at a distance of less than $100 h_{50}^{-1}$ Mpc, approximately in the direction of the Great-Attractor. Even though the cluster fails by more than an order of magnitude to provide the mass for the Great-Attractor effect, we may recall that similarly massive nearby clusters, Coma and Perseus, are found in the Great Wall superstructure and the Perseus-Pisces supercluster, respectively; two structures with estimated total masses on the order of $10^{16} M_{\odot}$. Therefore, the discovery of this massive cluster and its confirmation by X-ray observations may indeed suggest a way of finding additional massive structures contributing to the Great Attractor still hidden by the Milky Way.

We thank D. M. Neumann, S. Schindler, and M. Hirayama for helpful discussions and the ASCA-ANL and SimASCA software development teams and members of the ASCA team for making this study possible.

References

- Abell G. O., Corwin H. G., Olowin R. P. 1989, *ApJS* 70, 1
- Böhringer H., Neumann D. M., Schindler S., Kraan-Korteweg R. C. 1996, *ApJ* 467, 168
- Briel U. G., Henry J.P., Böhringer H. 1992, *A&A* 259, L31
- Burke B. E., Mountain R. W., Danies P. J., Dolat V.S. 1994, *IEEE Trans. Nuc. Sci.* 41, 375
- Burns J. O., Roettiger K., Ledlow M., Klypin A. 1994, *ApJ* 427, L87
- David L. P., Slyz A., Jones C., Forman W., Vrtilik D., Arnaud K. 1993, *ApJ* 412, 479
- Edge A. C., Stewart G. C. 1991, *MNRAS* 252, 428
- Ezawa H., Fukazawa Y., Makishima K., Ohashi T., Takahara F., Xu H., Yamasaki N. Y. 1998, *ApJ* 490, L33
- Fukazawa Y., Ohashi T., Fabian A. C., Canizares C. R., Ikebe Y., Makishima K., Mushotzky R.F., Yamashita K. 1994, *PASJ* 46, L55
- Fukazawa Y., Makishima K., Tamura T., Ezawa H., Xu H., Ikebe Y., Kikuchi K., Ohashi T. 1997, *PSAJ* 50, 187
- Hatsukade I. 1989, PhD Thesis, Osaka University
- Honda H., Hirayama M., Watanabe M., Kunieda H., Tawara Y., Yamashita K., Ohashi T., Hughes J. P., Henry J. P. 1996, *ApJ* 473, L71
- Koyama K., Takano S., Tawara Y. 1991, *Nature* 350, 135
- Kraan-Korteweg R. C., Woudt P. A., Cayatte V., Fairall A. P., Balkowski C., Henning P. A. 1996, *Nature* 379, 8
- Kulp K. 1998, Diploma Thesis, Universität München
- Lynden-Bell D., Faber S. M., Burstein D., Davies R. L., Dressler A., Terlevich R. J., Wegner G. 1988, *ApJ* 326, 19
- Ohashi T., Ebisawa K., Fukazawa Y., Hiyoshi K., Horii M., Ikebe Y., Ikeda H., Inoue H. et al. 1996, *PASJ* 48, 157
- Raymond J.C., Smith B.W. 1977, *ApJS* 35, 419
- Schindler S., Müller E. 1993, *A&A* 272, 137
- Serlemitsos P. J., Jalota L., Soong Y., Kunieda H., Tawara Y., Tsusaka Y., Suzuki H., Sakima T. et al. 1995, *PASJ* 47, 105
- Stark A.A., Gammie C.F., Wilson R.W., Bally J., Linke R.A., Heiles C., Hurwitz M. 1992, *ApJS*, 79, 77
- Tanaka Y., Inoue H., Holt S. S. 1994, *PASJ* 46, L37
- Xu H., Ezawa H., Fukazawa Y., Kikuchi K., Makishima K., Ohashi T., Tamura T. 1997, *PASJ* 49, 9

Vikhlinin A., Forman W., Jones C. 1997, ApJ 474, L7

White S. D. M., Briel U. G., Henry J. P. 1993, MNRAS 261, L8

Fig.1.

X-ray image of Abell 3627 taken with the GIS (GIS 2+GIS 3) in 0.7–10 keV, synthesized from two partially overlapping pointings. The image was smoothed using a Gaussian filter with $\sigma = 0'.5$, but not corrected for the XRT vignetting or partial shadows due to the detector support ribs. The contour levels are logarithmically spaced from 10^{-5} c s⁻¹/ pixel to 10^{-3} c s⁻¹/ pixel. The sky coordinates are J2000.

Fig.2.

Five regions from which the energy spectra were accumulated.

Fig. 3.

GIS spectrum (sum of the two detectors) of A3627 in (a) CENTER region and (b) SE region, shown together with the best-fit Raymond-Smith model and the fit residuals (see table 1).

Fig. 4.

SIS spectrum of A3627 in each region of figure 1, shown together with the best-fit Raymond-Smith model and the fit residuals (see table 1). The spectra from SIS-0 and SIS-1 are separately shown.

Table 1.. Results of the single-temperature Raymond-Smith model fits.*

‡	Pointing	Energy (keV)	Sensor	R^\sharp	N_{H} (10^{21}cm^{-2})	kT (keV)	A^\dagger	χ^2/ν
G-a	CENTER	0.7–10.0	G2+G3	14	1.0 (0.9–1.2)	6.7 (6.4–7.0)	0.16 (0.13–0.20)	134.6/104
S-a	CENTER	0.6–10.0	S0C1/S1C3	4.9	2.0 (1.9–2.1)	7.1 (6.8–7.5)	0.23 (0.17–0.29)	343.4/331
G-b	SE	0.7–10.0	G2+G3	14	0.7 (0.3–0.8)	5.1 (4.9–5.6)	0.25 (0.20–0.31)	111.0/104
S-b	SE	0.6–10.0	S0C2/S1C0	4.9	1.9 (1.6–2.1)	5.9 (5.4–6.7)	0.31 (0.20–0.45)	282.6/206
S-c	SE	0.6–10.0	S0C1/S1C3	4.9	1.3 (1.0–1.5)	5.2 (4.6–5.7)	0.27 (0.14–0.42)	202/179

* The error regions in parentheses refer to single-parameter 90% confidence limits.

‡ The region name in figure 2. The center of regions are G-a) $16^{\text{h}}14^{\text{m}}57^{\text{s}}, -60^{\circ}51'35''$, G-b) $16^{\text{h}}17^{\text{m}}28^{\text{s}}, -61^{\circ}4'10''$, S-a) $16^{\text{h}}14^{\text{m}}53^{\text{s}}, -60^{\circ}55'22''$, S-b) $16^{\text{h}}16^{\text{m}}50^{\text{s}}, -60^{\circ}58'20''$, and S-c) $16^{\text{h}}16^{\text{m}}34^{\text{s}}, -61^{\circ}9'36''$.

‡ The integrated radius in arcmin.

† Overall metallicity in solar unit mainly determined by the Fe-K line. Solar abundance ratios are assumed. The solar Fe/H ratio is taken to be 4.68×10^{-5} by number.

Fig.1

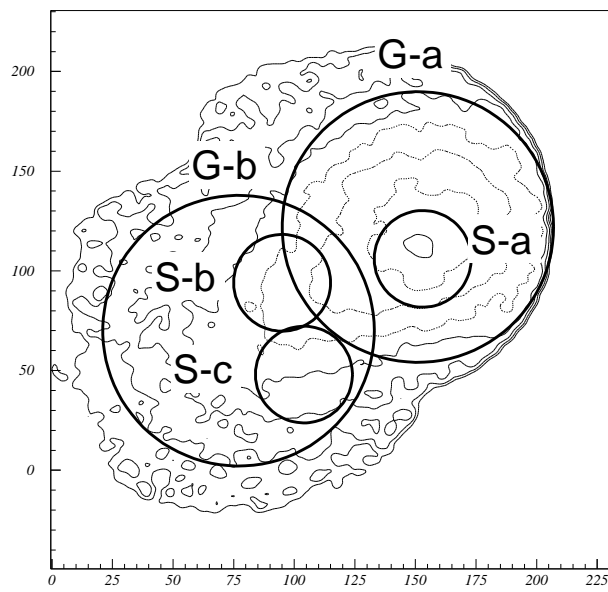
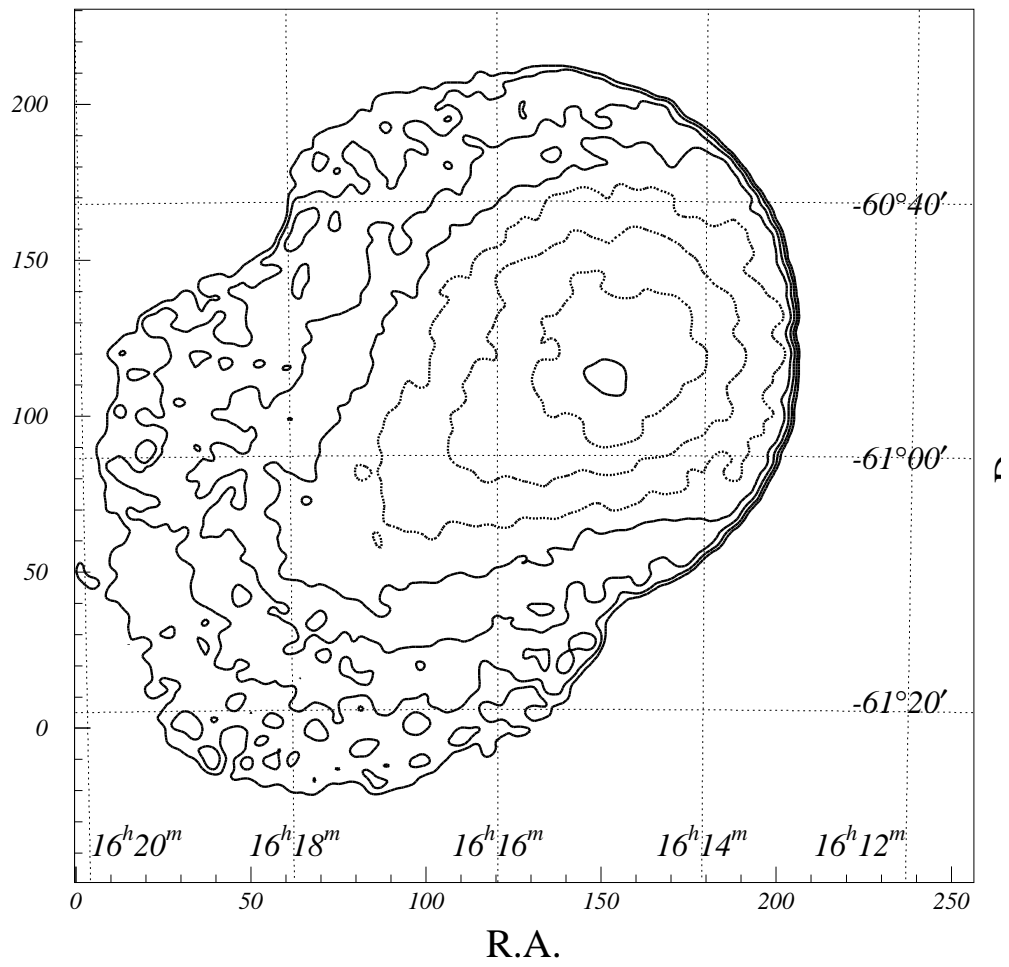


Fig.2

Fig.3

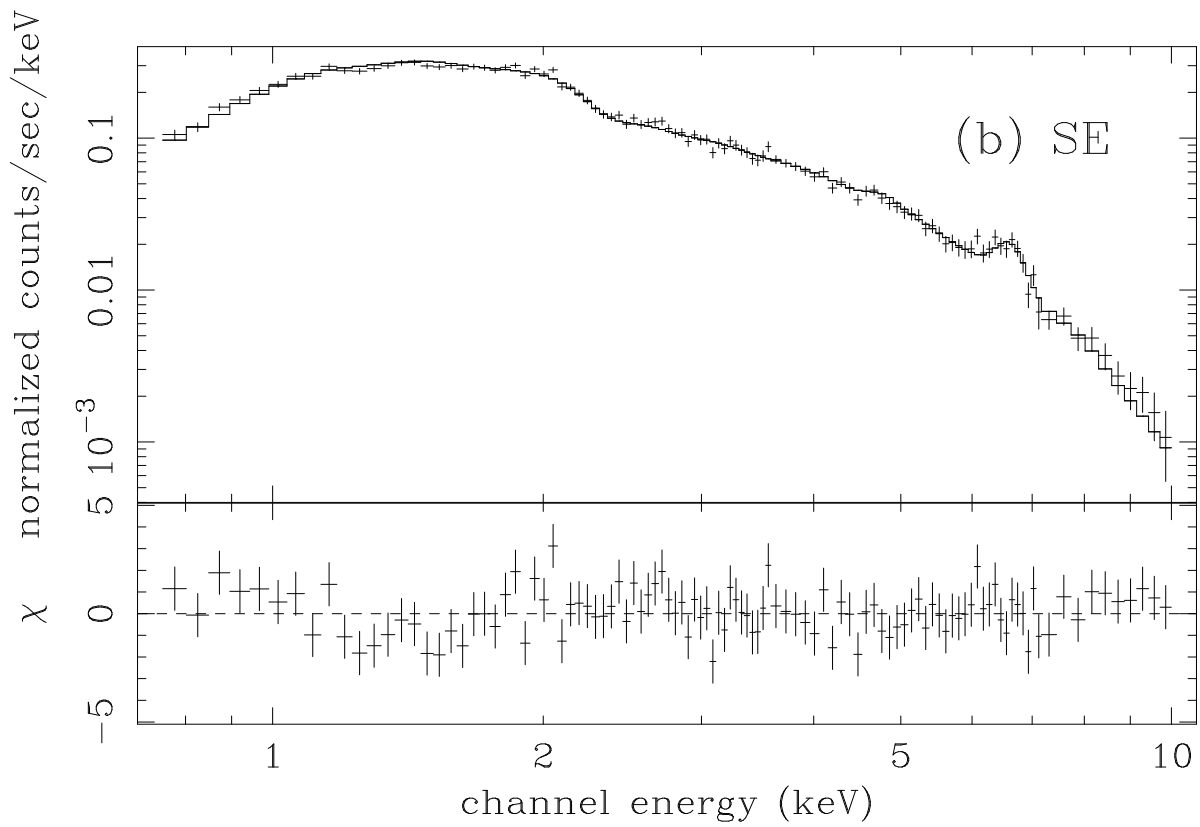
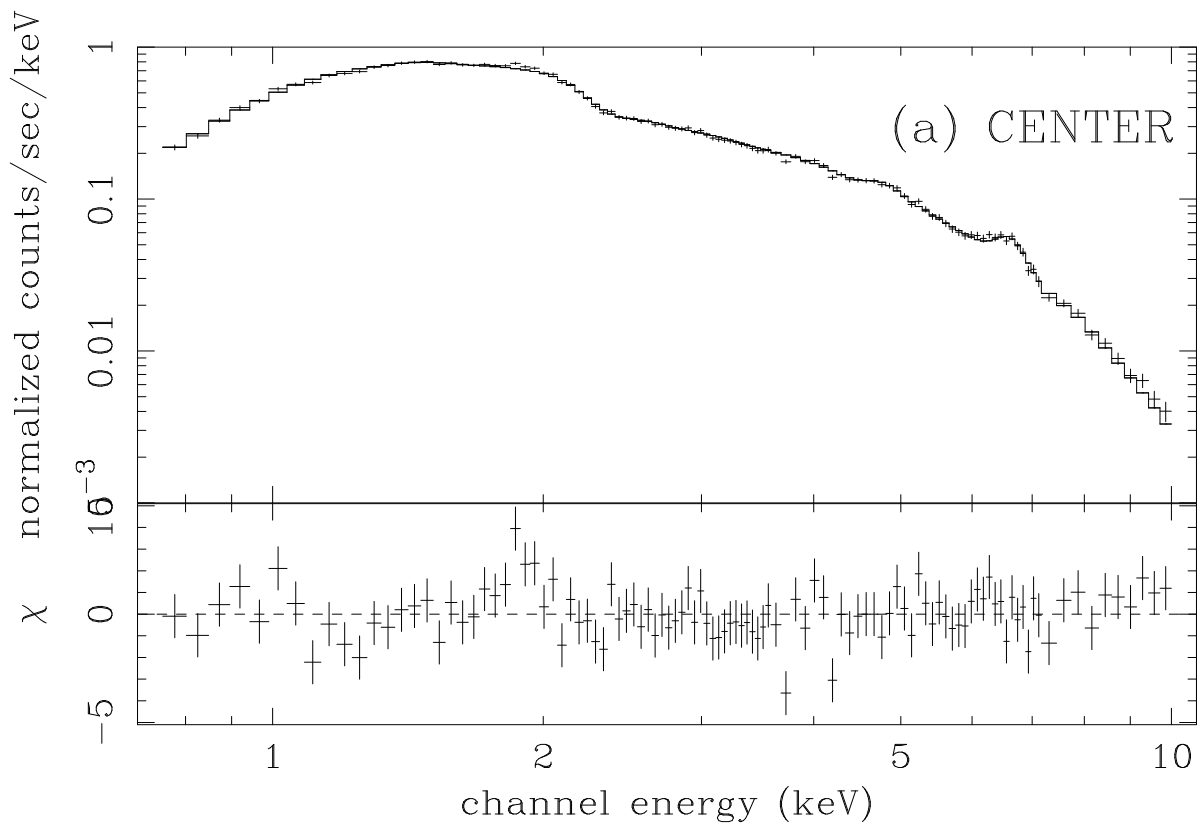


Fig.4

